Improving CAPRI Predictions: Optimized Desolvation for Rigid-Body Docking

Juan Fernández-Recio,[1†] Ruben Abagyan,[2] and Maxim Totrov[3*]
[1]*Department of Biochemistry, University of Cambridge, Cambridge, United Kingdom*
[2]*Department of Molecular Biology, The Scripps Research Institute, La Jolla, California*
[3]*Molsoft, LLC, La Jolla, California*

ABSTRACT **The ICM Docking and Interface Side-Chain Optimization (ICM-DISCO) showed promising predictive results during the first CAPRI experiment by successfully finding medium- or high-accuracy models in 3 of the 7 targets. A key factor was the ability to recognize near-native rigid-body geometries in a relatively low number of alternative docking poses, together with the successful refinement of the rigid-body docking interfaces. Since then, we have focused on improving the scoring function to optimally discriminate the near-native rigid-body conformations. For that, we have defined a new desolvation descriptor for rigid-body docking, based on atomic solvation parameters (ASPs) derived from octanol–water transfer experiments. This and other new approaches have been gradually incorporated into our docking procedure during our participation on the second CAPRI experiment. Overall, we produced reasonable models for 8 of the 9 official targets. Especially encouraging were those cases in which a homology model of 1 of the subunits had to be used during the docking simulations. And not less gratifying has been the successful prediction of antibody–antigen targets in a completely automatic, unrestrained fashion. In summary, our success rate (89%) shows a consistent improvement over the previous CAPRI rounds, and suggests that a correct desolvation description is key for improved protein–protein docking predictions. Proteins 2005;60:308–313.** © 2005 Wiley-Liss, Inc.

INTRODUCTION

Interest in protein docking is growing within the scientific community, and many interdisciplinary approaches are being applied to model, predict, and understand protein–protein interactions, a major challenge in structural biology. The CAPRI experiment (http://capri.ebi.ac.uk), in Rounds 1 and 2,[1] showed a good overview of the state of the art of the different docking methods and their limitations. Our approach, the ICM Docking and Interface Side-Chain Optimization (ICM-DISCO), succeeded in finding medium- or high-accuracy models in 3 of the 7 targets.[2] A key factor was the ability to recognize near-native rigid-body geometries in a relatively low number of alternative docking poses. The rigid-body approach was widely spread among the docking methods as a first sampling step that very often provides near-native docking interfaces, since changes upon binding are often small.[3–6] Our rigid-body first step used ICM pseudo-Brownian optimization[7,8] of binding potentials precalculated on a 3-dimensional (3D) grid. It was originally benchmarked on 24 unbound–unbound pairs[9] and was later optimized and extended to unrestricted global docking.[10] The rigid-body docking was followed by the refinement of the solutions and final scoring, which included specific filtering criteria [e.g., number of contacts in the antibody complementarity defining regions (CDRs)] on a case-by-case basis.

After the lessons learned during the first CAPRI, we have focused on improving the scoring function in order to optimally discriminate the near-native rigid-body conformations. A new desolvation descriptor, based on atomic solvation parameters (ASPs) derived from octanol–water transfer experiments, was optimized for rigid-body docking.[10] The global docking energy landscapes generated with the new energy function showed a clear funnel shape around the known binding sites. Indeed, a systematic analysis of protein surfaces using the new ASP-based desolvation identified optimal docking areas (ODAs) that corresponded to known protein binding sites in more than 80% of the cases.[11] We have gradually incorporated these new approaches into our docking procedure during our participation in the latest rounds of the CAPRI experiment. These improvements increased the automation of the method and dramatically reduced (often to zero) the amount of user input needed for accurate docking predictions. Furthermore, 2 of the targets (9 and 10) involved modeling of oligomeric structures. An unusual characteristic of these systems is the symmetry. Symmetry can be included in the modeling protocol as an external constraint, either through postfiltering of the docking solutions or through an energy penalty term that forces the system into symmetric configuration. We, on the other hand, attempted to impose symmetry as an intrinsic feature of the model, so that only symmetric configurations can be realized throughout the course of the docking procedure.

Grant sponsor: Marie Curie Research Fellowship (to J. Fernández-Recio).

[†]Current address: Molecular Modelling and Bioinformatics Unit, IRBB-PCB, C/Josep Samitier 1-5, Barcelona 08028, Spain

*Correspondence to: Maxim Totrov, Molsoft, LLC, 3366 Torrey Pines Court, Suite 300, La Jolla, CA 92037. E-mail: max@molsoft.com

Received 24 January 2005; Accepted 10 March 2005
DOI: 10.1002/prot.20575

Here we report our results in CAPRI Rounds 3–5. Overall, our docking approaches predicted acceptable- to high-accuracy models for 8 of the 9 targets.

METHODS

ICM-DISCO: Rigid-body Docking and Interface Side-Chain Optimization

The ICM-DISCO protein–protein docking method was used in CAPRI Rounds 1 and 2.[2] It is based on the ICM pseudo-Brownian minimization[7,8] and biased probability side-chain optimization[12] with binding potentials[13,14] precalculated on a 3D grid.[9,15] The atomic accessible surface area (ASA)-based solvation energy[16] is added to the binding energy to revaluate the rigid-body docking solutions. Then, the 400 lowest energy rigid-body docking solutions are clustered[17] and further optimized by the ICM-DISCO refinement step.[2]

Total computational times for the rigid-body docking step ranged from 70 min on 20 Pentium-4 2.4 GHz Linux CPUs (Target 11) to 28 h on 46 CPUs (Target 14). For the refinement step, times ranged from 70 min on 16 CPUs (Target 11) to 30 h on 11 CPUs (Target 14).

New Scoring of Rigid-Body Solutions in CAPRI Round 5

By the time of CAPRI Round 5, we had devised a new scoring function for rigid-body docking that largely improved the docking energy landscapes.[10] This scoring function [Eq. (1)] comprised van der Waals, electrostatics, and hydrogen bonding energy, plus a new ASA-based desolvation adjusted for optimal rigid-body docking[11]:

$$E = 0.40E_{\mathrm{vw(max\ 1.0)}} + E_{\mathrm{ele}} + 2.43E_{\mathrm{hb}} + E_{\mathrm{solv}}^{\mathrm{RigBodDock}}. \quad (1)$$

We applied this optimized energy function to score the rigid-body docking poses of the 3 targets in Round 5. For Targets 18 and 19, we did not even use any refinement step, as we were satisfied with the ranking obtained by the new scoring function.

Modeling of Symmetric Oligomers in Targets 9 and 10

For Targets 9 and 10, a protocol different from our standard procedure was designed to account for the symmetry of the complexes. The approach takes advantage of the feature of internal coordinate modeling framework that allows us to group several internal variables as "dependent." In the most simple case, this dependency is an equality; that is, the variables in the group always have the same value and effectively are considered as one. Thus, if the system comprises several identical molecules (monomers of the oligomeric structure), by grouping all corresponding internal variables across the monomers, we can keep all subunits in the identical conformation at all times.

Furthermore, the position of the molecule in space is controlled in the ICM representation by 6 special internal variables, including 5 "virtual" angles and 1 "virtual" bond length. The first of these "'virtual" angles (ϕ_{vtI}) defines the rotation of the molecules around the Z coordinate axis (Fig. 1). Therefore, for 2 subunits related by a rotation around the Z axis, all internal coordinates will be identical except for this "virtual" torsion. This observation suggest that C_n oligomers can be simulated very efficiently by grouping the corresponding variables in all subunits except for the first "virtual" torsion (ϕ_{vtI}). The latter is set to 0 for the first subunit, $360/n$ for the second, and so on. The second "virtual" variable (θ_{vtI}) is also kept constant, which effectively prevents the oligomer from moving as a whole along the Z axis. By changing the remaining 4 "virtual" internal variables, all possible oligomeric configurations can be sampled while variable linking continuously maintains axial C_n symmetry. Similarly, internal flexibility of the subunits can be sampled by changing appropriate internal variables (χ_i torsion for side-chain flexibility, ϕ/ψ pairs for the backbone flexibility), and again linking will automatically preserve symmetry and identical conformations between the subunits.

RESULTS

Target 8 (Bound Nidogen-G3–Unbound Laminin)

During rigid-body docking, the bound nidogen-G3 was considered the static molecule (receptor), while the unbound laminin was the moving one (ligand). Laminin is formed by 3 epidermal growth factor (EGF)-like domains [Protein Data Bank (PDB) code: 1KLO]. Although nidogen-G3 was known to bind mostly, but not necessarily exclusively, to the middle domain of laminin (residues 65–120), we used the whole laminin molecule for docking. The 400 lowest energy rigid-body docking solutions were clustered and subjected to interface side-chain refinement. We found in the literature the existence of a laminin binding loop in nidogen (residues 71–77; sequence NIDPNAV). Based on that, rigid-body docking conformation rank 41 looked particularly good (the binding loop was buried in the interface), so we decided to include it as our model number 1. The remaining submitted models (2 to 10) were defined by the rank obtained after refinement. When the X-ray complex structure was released, we found that our model 1 [Fig. 2(a)] had 35 % of correct contacts and 1.4 Å of interface root-mean-square deviation (RMSD) with respect to the experimental complex.

Target 9 (Wild-Type LicT Homodimer—to be Rebuilt From a Different Mutant Dimer)

The inspection of the subunit structure suggested flexibility of the linker loop N166–M169 between the 2 subdomains. In our Monte Carlo (MC) simulations we therefore allowed the $\phi/\psi/\chi$ angles for the residues 166–169 to change, along with the 4 positional virtual variables. Linking the corresponding variables maintained both subunits in identical conformations and allowed them to change simultaneously. First torsions were kept at 0° and 180°, and one other virtual variable was kept fixed, because it controls translation along the axis of the oligomer and is therefore redundant (does not result in new oligomeric configurations). Best low-energy conformations generated in 8 independent MC runs were submitted. Unfortunately, we later found from the experimental structure that while we correctly guessed that the rear-

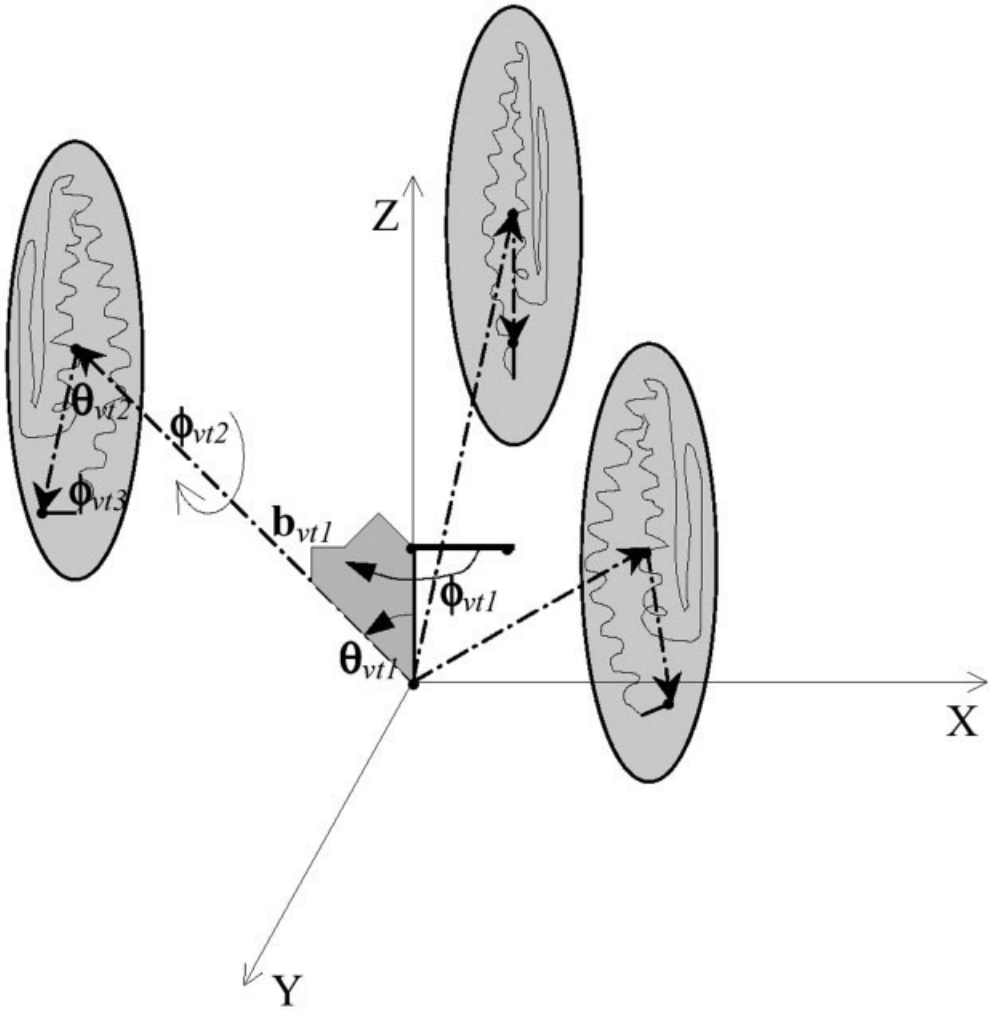

Fig. 1. Schematic diagram of the internal coordinates tree for an oligomeric system. Six "virtual" internal variables, dihedrals ϕ_{vt1}, ϕ_{vt2}, ϕ_{vt3}, planar angles θ_{vt1}, θ_{vt2}, and a virtual bond length b_{vt1} define the position of a molecule (subunit). Note that the first dihedral ϕ_{vt1} defines rotation around the *Z* coordinate axis; therefore, by definition, in any axially symmetrical arrangement around *Z* axis, the subunits should have all corresponding internal variables equal, with the exception of ϕ_{vt1}.

rangement of the 2 subdomains within monomers is essential for the formation of the native structure, the flexible linker region is in fact more extensive (residues L165:N171) and the required domain movement could not be reproduced with only 4 residues allowed to flex in our simulations.

Target 10 [Tick-Borne Encephalitis Virus (TBEV) Envelope Protein Trimer—to be Rebuilt From Dimer]

For Target 10 simulations, the information provided by crystallographers suggested that the protein forms a trimeric structure (available structure was a dimer), and that the C-terminal domain does not play important role in subunit interactions and therefore does not need to be considered. Thus, we utilized the approach described in methods by generating 3 copies of truncated monomer, linking all but the first internal variable across the 3 monomers and setting the first internal variable to 0°, 120°, and 240°, respectively. The 4 remaining "virtual" variables were subjected to global optimization by the MC minimization procedure. After removal of similar conformations, we submitted the 10 lowest energy solutions from the combined results of 5 independent MC simulations. Solution number 2 turned out to be one of the very few acceptable models for this target [Fig. 2(b)], with 15% of correct native contacts and 4.5 Å interface RMSD with respect to the experimental trimeric structure (PDB code: 1URZ).[18]

Target 11 (Unbound Cohesin–Homology-Modeled Dockerin)

The structure of dockerin was built by comparative modeling based on the NMR structure of a homologous dockerin (PDB code: 1DAQ) with 48% sequence identity. We used the ICM-Homology software (www.molsoft.com)

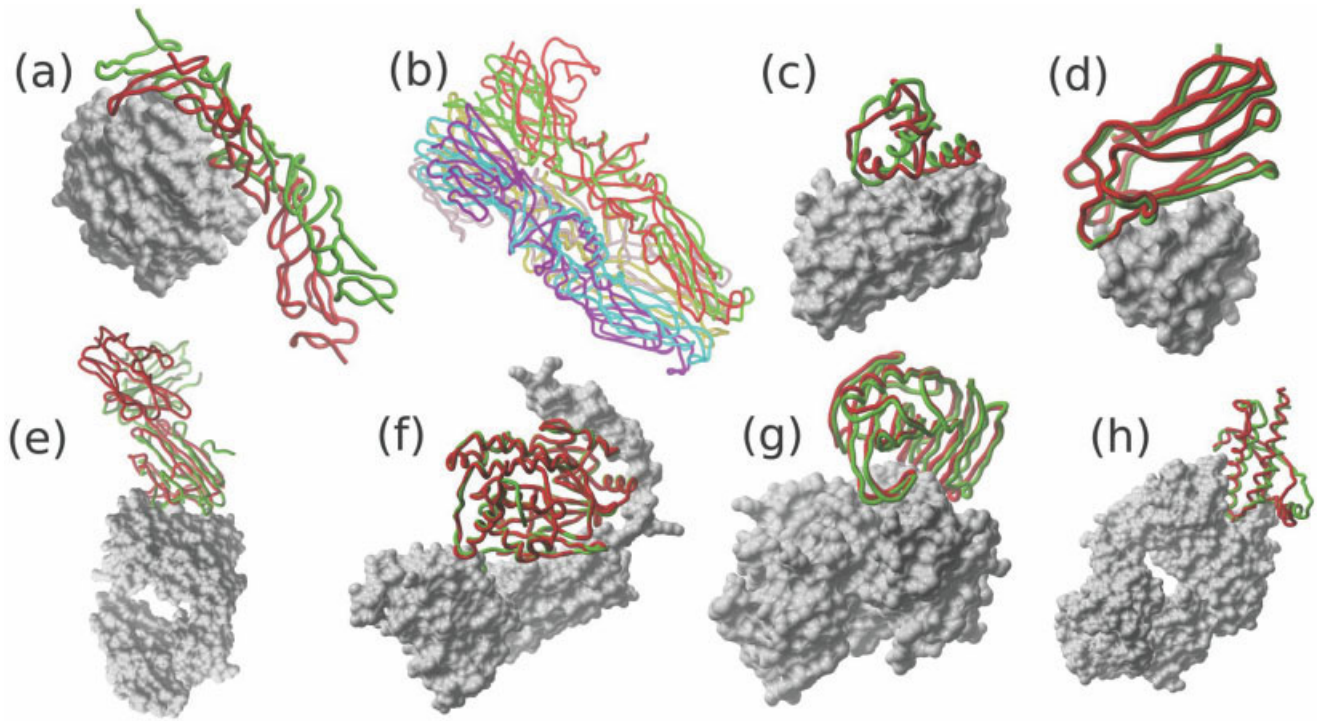

Fig. 2. Representation of our best submitted models for Targets 8 (**a**), 10 (**b**), 11 (**c**), 12 (**d**), 13 (**e**), 14 (**f**), 18 (**g**), and 19 (**h**). The ligand backbone is represented in red, and the receptor molecular surface is in white. The position of the ligand in the complex X-ray structure is represented in green (after superimposing the receptor molecules). For Target 10 (b), the 3 monomers in the trimeric submitted model are shown in red, pink, and magenta, respectively, superimposed onto the trimeric X-ray structure (whose monomer subunits are shown in green, yellow, and cyan, respectively).

for the building of the model and further refinement by side-chain and loop optimization. In the docking simulations, the receptor was the unbound cohesin (PDB code: 1ANU), and the ligand the homology-based model of dockerin. The 400 lowest energy solutions were clustered and subjected to interface side-chain refinement. No other filtering criteria were used, and the 10 lowest energy refined solutions were submitted. Our model number 3 was quite close to the experimental complex structure (PDB code: 1OHZ),[19] with 35% of correct contacts and 1.2 Å of interface RMSD [Fig. 2(c)].

The docking results for this target were highly encouraging. The method automatically found a near-native solution ranked third, which is indeed remarkable if we consider that this target comprised several challenges that are often found in real docking problems: use of unbound structures, homology models, and NMR coordinates. Our results show that realistic predictions are possible from completely automatic docking without any additional user input.

Target 12 (Unbound Cohesin–Bound Dockerin)

The structure of dockerin was now taken from the complex (PDB code: 1OHZ), randomly oriented, and we used it as the receptor. Ligand was unbound cohesin, as in Target 11 (PDB code: 1ANU). The 400 lowest energy rigid-body docking solutions were clustered and refined. No other filtering criteria were used, and the 10 lowest energy refined solutions were submitted. Our model number 1 was very close to the experimental complex structure (PDB code: 1OHZ),[19] with 80% of correct contacts, 0.7 Å of ligand RMSD, and 0.3 Å of interface RMSD [Fig. 2(d)].

The high quality of our best model was certainly striking; even better, it was automatically ranked 1 by our scoring function. Although this was an unbound–bound target and therefore it cannot be considered a completely "real-life" situation, these good results prove that our sampling and scoring functions performed optimally.

Target 13 [Unbound Surface Antigen 1 (SAG1)–Bound Antibody)

We used as receptor the bound antibody, and as ligand, the unbound SAG1 (PDB code: 1KZQ). The resulting 12,149 conformations were filtered according to the CDR contact ratio (ratio = number of CDR contacts/number of total contacts) on the antibody. A total of 1027 solutions with ratio of more than 0.5 were selected. From this selection, the 400 solutions with the lowest energy values were clustered and subjected to interface side-chain refinement. The 10 lowest energy solutions after refinement were submitted to CAPRI. Our model number 6 [Fig. 2(e)], predicted 23% of the native contacts and had 2.5 Å RMSD with respect to the X-ray structure of the complex.

During CAPRI Round 4, we were still testing our newly developed scoring function [Eq. (1)]. After the complex structure was released, we revaluated the 12,149 original rigid-body docking solutions with this function, and we found that the lowest energy solution (rank 1) was 3.6 Å

ligand RMSD from the experimental structure. It is remarkable that this was obtained automatically by the new scoring function, without needing the CDR contact ratio or any other filtering. We decided at this point to use the new scoring function in all future docking calculations, and the first test was CAPRI Round 5.

Target 14 [Homology-Modeled Protein Phosphatase 1-β–Bound Myosin Phosphatase–Targeting Subunit (MYPT1)]

The structure of protein phosphatase 1-β was built by ICM-Homology based on the NMR structure of the homologous protein phosphatase 1-α (PDB code: 1FJM), of 93% sequence identity. In the docking simulations, the receptor was the bound MYPT1, and the ligand, the homology model of the phosphatase. The rigid-body docking solutions were sorted by the recently developed scoring function [Eq. (1)]. The 400 lowest energy solutions were clustered and refined. We have to emphasize that we did not use any other filtering criteria or additional information; thus, the 10 lowest energy refined solutions were automatically selected by our scoring function and submitted to CAPRI. Our model number 1 was very close to the experimental complex structure (PDB code: 1S70),[20] with 61% of correct contacts, 0.6 Å of ligand RMSD, and 0.4 Å of interface RMSD [Fig. 2(f)]. This model had the highest percentage of correct native contacts (like Baker's one) and the lowest ligand RMSD among the models submitted by all participants. Similarly to Target 11, this case implied the additional challenge of using a homology-based model. Our method thus consistently yielded good results when using homology models as input structures for docking.

Target 18 [Unbound Xylanase–Bound *Triticum aestivum* Xylanase Inhibitor (TAXI)]

We used the bound TAXI as the receptor, and the unbound xylanase (PDB 1UKR) as the ligand. The resulting rigid-body docking solutions were ranked by the new scoring function [Eq. (1)]. We applied a final filtering by selecting only those docking solutions in which at least 1 nonhydrogen TAXI atom was found within 6 Å from the xylanase active site (Glu79, Glu170, as defined in the xylanase SwissProt entry named XYN1_ASPNG, code P55329). After the filtering, we submitted the 10 lowest energy solutions. We found 2 near-native solutions within our submissions, ranked 4 and 9. The best of them was model number 9 [Fig. 2(g)], with 66% of correct contacts, 3.0 Å of ligand RMSD, and 1.4 Å of interface RMSD with respect to the experimental complex. This was the model with the lowest ligand and interface RMSD of all participants in this target.

Target 19 (Homology-Modeled Prion–Bound FAB)

The structure of the ovine prion was built by ICM-Homology, based on the NMR structure of the homologous bovine prion (PDB code: 1DWY) of 95% sequence identity. In the docking simulations, the receptor was the bound FAB, and the ligand, the homology model of the prion. The rigid-body docking solutions were sorted by the recently developed scoring function [Eq. (1)]. No other filtering criteria, restraints, or additional information were used, and the 10 lowest energy solutions were directly submitted to CAPRI. Our model number 4 was close to the experimental complex structure (PDB code: 1TPX),[21] with 74% of correct contacts, and 1.0 Å of interface RMSD [Fig. 2(h)]. This model had the highest percentage of correct native contacts (like Baker's one) of all participants. Similarly to Targets 11 and 14, our method yielded consistently good results when using homology models as input structures for docking.

DISCUSSION AND CONCLUSIONS

We have participated in all 9 official targets in CAPRI Rounds 3–5. In 7 targets, we have applied our automatic protein docking procedure, which has been gradually improved along these CAPRI rounds. In all these cases, the procedure found a near-native solution within the 10 submitted models. In addition, for 2 of the targets, we had to devise a variation of our docking tools. It is remarkable that this "ad hoc" approach gave a near-native solution in at least 1 of these 2 cases (Target 10). Overall, our results in these CAPRI Rounds 3–5 show a consistent improvement with respect to previous tests: A near-native solution was found in 44%, 78%, and 89% of the cases within the top 1, 5, and 10 solutions, respectively (Table I). Actually, we were the only group that submitted acceptable- to high-accuracy models for all targets but one. The most exciting consequence of our CAPRI results is that the use of desolvation optimized for rigid-body docking was able to dramatically improve the rank of near-native solutions from the very early rigid-body docking stages. Although it was tested before, this scoring function was first used in CAPRI Round 5, with excellent results. Especially, in the 2 latest targets (18 and 19) we did not need to apply the refinement step at all, since the rigid-body docking already yielded correctly ranked near-native solutions. It is also noticeable that for the antibody–antigen in Target 19, we did not need to use any CDR-based restraint or filtering. This suggests that more efforts toward improving the rigid-body docking step, and in particular, the treatment of desolvation upon binding, could lead to a better selection of near-native solutions, so that a reduced effort in refinement may be needed in some cases.

We also developed a modification of the internal coordinate representation with dependent variable groups, which allows very efficient treatment of oligomers with axial symmetry, effectively reducing the configurational space to only 4 degrees of freedom in the case of rigid-body docking. Furthermore, for flexible docking, the monomeric subunits are automatically maintained in the same internal conformation.

In summary, our experience with CAPRI has been highly rewarding, and the experiment continues to be an enriching experience that is progressively improving our approach to protein–protein docking.

ACKNOWLEDGMENTS

Our thanks to the organizers and evaluators of the CAPRI experiment, and the scientists that provided the

TABLE I. Best Models Submitted by Our Group for Each CAPRI Target

Target number	Receptor–ligand	Model[a]	% correct contacts	ligand RMSD[b]	Interface RMSD[c]	Quality[d]	Additional filtering
08	Nidogen G3–laminin (bound–unbound)	1	35	7.6	1.4	**	Laminin binding loop
09	Wild-type LicT homodimer (from different mutant dimer)	1	1	26.7	19.6	—	No
10	TBEV envelope protein trimer (from dimer)	2	15	8.5	4.5	*	No
11	Cohesin–dockerin (unbound–homology model)	3	35	6.0	1.2	**	No
12	Cohesin–dockerin (unbound–bound)	1	80	0.7	0.3	***	No
13	SAG1–antibody (unbound–bound)	6	23	11.1	2.5	*	CDR contacts
14	Protein phosphatase 1-β–MYPT1 (homology model–bound)	1	61	0.6	0.4	***	No
18	Xylanase–TAXI (unbound–bound)	9	66	3.0	1.4	**	Active site distance
19	Prion–FAB (homology model–bound)	4	74	4.1	1.0	**	No

[a]Rank of the best model in our 10 submissions for each target.
[b]RMSD with respect to the X-ray structure, calculated for the C^{α} atoms of the ligand residues when only the receptor molecules (model and X-ray structure) are superimposed.
[c]RMSD with respect to the X-ray structure, calculated for the C^{α} atoms of the receptor and ligand interface residues.
[d]Quality of the models as evaluated by the organizers (*acceptable; ** medium accuracy; *** high accuracy).

target structures, for their time, effort, and patience. We are also grateful to Prof. Tom Blundell for helpful discussions and for the use of the IBM Linux cluster in the Department of Biochemistry of the University of Cambridge for some of the calculations.

REFERENCES

1. Méndez R, Leplae R, De Maria L, Wodak SJ. Assessment of blind predictions of protein–protein interactions: current status of docking methods. Proteins 2003;52:51–67.
2. Fernández-Recio J, Totrov M, Abagyan R. ICM-DISCO docking by global energy optimization with fully flexible side-chains. Proteins 2003;52:113–117.
3. Conte LL, Chothia C, Janin J. The atomic structure of protein–protein recognition sites. J Mol Biol 1999;285:2177–2198.
4. Norel R, Petrey D, Wolfson HJ, Nussinov R. Examination of shape complementarity in docking of unbound proteins. Proteins 1999;36:307–317.
5. Vakser IA, Matar OG, Lam CF. A systematic study of low-resolution recognition in protein–protein complexes. Proc Natl Acad Sci USA 1999;96:8477–8482.
6. Smith GR, Sternberg MJ. Prediction of protein–protein interactions by docking methods. Curr Opin Struct Biol 2002;12:28–35.
7. Abagyan R, Totrov M, Kuznetsov D. ICM—a new method for structure modeling and design: applications to docking and structure prediction from the distorted native conformation. J Comp Chem 1994;15:488–506.
8. Totrov M, Abagyan R. Detailed ab initio prediction of lysozyme–antibody complex with 1.6 Å accuracy. Nat Struct Biol 1994;1:259–263.
9. Fernández-Recio J, Totrov, M., Abagyan, R. Soft protein–protein docking in internal coordinates. Protein Sci 2002;11:280–291.
10. Fernández-Recio J, Totrov M, Abagyan R. Identification of protein–protein interaction sites from docking energy landscapes. J Mol Biol 2004;335:843–865.
11. Fernández-Recio J, Totrov M, Skorodumov C, Abagyan R. Optimal docking area: a new method for predicting protein–protein interaction sites. Proteins 2005;58:134–143.
12. Abagyan R, Totrov M. Biased probability Monte Carlo conformational searches and electrostatic calculations for peptides and proteins. J Mol Biol 1994;235:983–1002.
13. Totrov M, Abagyan R. Flexible protein–ligand docking by global energy optimization in internal coordinates. Proteins 1997;Suppl 1:215–220.
14. Goodford PJ. A computational procedure for determining energetically favorable binding sites on biologically important macromolecules. J Med Chem 1985;28:849–857.
15. Totrov M, Abagyan R. Protein–ligand docking as an energy optimization problem. In: Raffa RB, Editor. Drug-receptor thermodynamics: introduction and applications. New York: Wiley; 2001. p 603–624.
16. Wesson L, Eisenberg D. Atomic solvation parameters applied to molecular dynamics of proteins in solution. Protein Sci 1992;1:227–235.
17. Abagyan R, Argos P. Optimal protocol and trajectory visualization for conformational searches of peptides and proteins. J Mol Biol 1992;225:519–532.
18. Bressanelli S, Stiasny K, Allison SL, Stura EA, Duquerroy S, Lescar J, Heinz FX, Rey FA. Structure of a flavivirus envelope glycoprotein in its low-pH-induced membrane fusion conformation. EMBO J 2004;23:728–738.
19. Carvalho AL, Dias FM, Prates JA, Nagy T, Gilbert HJ, Davies GJ, Ferreira LM, Romao MJ, Fontes CM. Cellulosome assembly revealed by the crystal structure of the cohesin–dockerin complex. Proc Natl Acad Sci USA 2003;100:13809–13814.
20. Terrak M, Kerff F, Langsetmo K, Tao T, Dominguez R. Structural basis of protein phosphatase 1 regulation. Nature 2004;429:780–784.
21. Eghiaian F, Grosclaude J, Lesceu S, Debey P, Doublet B, Treguer E, Rezaei H, Knossow M. Insight into the PrPC→PrPSc conversion from the structures of antibody-bound ovine prion scrapie-susceptibility variants. Proc Natl Acad Sci USA 2004;101:10254–10259.